

## Precursory Cooper flow in ultralow-temperature superconductors

Pengcheng Hou <sup>1,3,\*</sup> Xiansheng Cai <sup>2,\*</sup> Tao Wang <sup>1</sup> Youjin Deng <sup>1,3,4</sup> Nikolay V. Prokof'ev, <sup>2</sup>  
Boris V. Svistunov <sup>1,5</sup> and Kun Chen <sup>6,7,†</sup>

<sup>1</sup>Department of Modern Physics, University of Science and Technology of China, Hefei, Anhui 230026, China

<sup>2</sup>Department of Physics, University of Massachusetts, Amherst, Massachusetts 01003, USA

<sup>3</sup>Hefei National Laboratory, University of Science and Technology of China, Hefei 230088, China

<sup>4</sup>MinJiang Collaborative Center for Theoretical Physics, College of Physics and Electronic Information Engineering, Minjiang University, Fuzhou 350108, China

<sup>5</sup>Wilczek Quantum Center, School of Physics and Astronomy, Shanghai Jiao Tong University, Shanghai 200240, China

<sup>6</sup>Center for Computational Quantum Physics, Flatiron Institute, 162 5th Avenue, New York, New York 10010, USA

<sup>7</sup>CAS Key Laboratory of Theoretical Physics, Institute of Theoretical Physics, Chinese Academy of Sciences, Beijing 100190, China



(Received 7 March 2023; revised 13 September 2023; accepted 15 December 2023; published 26 January 2024)

Superconductivity at low temperature—observed in lithium and bismuth, as well as in various low-density superconductors—calls for the development of reliable theoretical and experimental tools for predicting ultralow critical temperatures  $T_c$  of Cooper instability in a system demonstrating simply normal Fermi liquid behavior in a broad range of temperatures below the Fermi energy  $T_F$ . Equally important are controlled predictions of stability in a given Cooper channel. We identify such a protocol within the paradigm of precursory Cooper flow—a universal ansatz describing logarithmically slow temperature evolution of the linear response of the normal state to the pair-creating perturbation. Applying this framework to the two-dimensional uniform electron gas, we reveal a series of exotic superconducting states, pushing controlled theoretical predictions of  $T_c$  to the unprecedentedly low scale of  $10^{-100} T_F$ .

DOI: 10.1103/PhysRevResearch.6.013099

### I. INTRODUCTION

The conceptual elegance of the Kohn-Luttinger theorem establishing that the Fermi liquid state is unstable in high-angular momentum Cooper channels at low temperatures comes at the price of lacking accurate predictions as to which channels get unstable first and at what temperatures. Experimentally, each new discovery of the ultralow-temperature superconductor, be it lithium [1] or bismuth [2], exhibiting superconductivity at about 0.1 mK, emerges as a surprise. The potential for observing analogous phenomena in traditionally nonsuperconducting metals such as gold, copper, or sodium, as well as in low-density superconductors [3–5], adds to the scientific intrigue, with no *a priori* knowledge of the critical temperature  $T_c$  that one should expect for a given system.

There is, however, a fundamental reason to expect that the desired answers can be controllably extracted—definitely theoretically and, hopefully, experimentally as well—from the system's properties in the normal Fermi liquid regime at temperatures much lower than the Fermi energy  $T_F$ , but still many orders of magnitude higher than  $T_c$ . Indeed, the (ultra-)low

value of  $T_c$  is due to the emergent Bardeen-Cooper-Schrieffer (BCS) regime of instability, when the system that is strongly correlated at the ultraviolet level gets renormalized into the Fermi liquid with a weak effective BCS interaction characterized by a dimensionless negative coupling constant  $|g| \ll 1$ . The result is an exponentially small critical temperature,  $T_c \sim T_F e^{-1/|g|}$ . The BCS nature of the transitions implies a rather characteristic temperature evolution of the pair susceptibility,  $\chi_0(T)$ , defined as the linear response to a static pair-creating perturbation. On the approach to the critical point,  $\chi_0(T)$  should behave as [6,7]

$$\chi_0(T) \propto 1/\ln(T/T_c) \quad (T \rightarrow T_c + 0). \quad (1)$$

Experimental studies across a range of superconductors have validated this prediction using superconductor-superconductor tunnel junctions [8–13].

While providing a proof-of-principle result for the idea of extracting  $T_c$  from properties of the normal state at  $T \gg T_c$ , relation (1) turns out to be rather impractical, and sometimes even misleading, when it comes to a controlled quantitative analysis of (in)stability in a given pairing channel (for an illustration, see the blue curve in Fig. 1). The reason is that ansatz (1) ignores a logarithmic prefactor (its physical origin is discussed below) that is slowly evolving with temperature, making a naïve extrapolation of an apparent linear dependence of  $1/\chi_0(T)$  on  $\ln T$  from high temperature to the temperature when it is supposed to hit zero very inaccurate, not to mention that it may predict finite  $T_c$  for a Cooper-stable channel (see a similar discussion in Ref. [14]).

\*These authors contributed equally to this paper.

†chenkun@itp.ac.cn

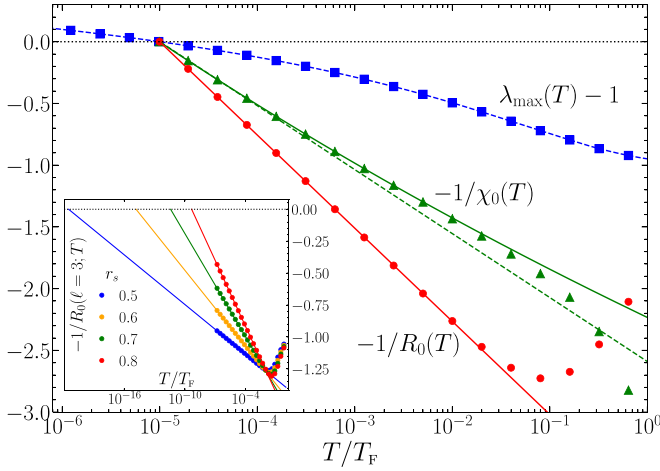


FIG. 1. Finite-temperature flows of the largest  $s$ -wave eigenvalue,  $\lambda_{\max}$ , of the standard gap function equation (blue squares connected by line) and linear response functions  $\chi_0$  (green triangles) and  $R_0$  (red circles) computed for the 2D UEG at  $r_s = 1.156$ . The  $1/\chi_0$  and  $1/R_0$  data are fitted using Eqs. (2) and (3), demonstrating excellent agreement. The role of the logarithmic numerator in Eq. (2) is clearly visible as the difference between the solid green line [fitted with ansatz (2)] and the dashed green line [fitted with ansatz (1)]. The  $1/\chi_0$  and  $1/R_0$  flows undergo qualitative changes near  $T/T_F \sim 10^{-1}$ , where  $T_F$  is the Fermi temperature; this sets an energy scale  $\Lambda$  below which the attractive Cooper-channel interaction emerges.

Recently, a numeric method—the so-called implicit renormalization (IR)—allowing one to accurately predict  $T_c$  from the field-theoretical properties of the system at  $T \gg T_c$  was proposed in Ref. [14] and further developed in Refs. [15,16], with an application to the model of uniform electron gas. Despite unquestionable success, the IR approach encounters certain technical limitations and lacks a direct connection with what can be measured experimentally. Technical limitations of IR are most pronounced in the vicinity of the “quantum transition point” (QTP) at which a given channel undergoes a transition from a Cooper-stable to Cooper-unstable regime. It is thus crucial to find an approach that is complementary to the IR and one compatible with experimental protocols.

In this paper, we show that the desired solution is simply provided by an expression that is more accurate than (2), but still physically transparent, for the pair susceptibility. Specifically, we find that the following three-parametric ansatz (universal to all ultralow-temperature BCS-type superconductors)—the *precursory Cooper flow* (PCF) ansatz—perfectly captures the temperature evolution of  $\chi_0$  within a broad temperature range:

$$\chi_0 = \frac{c \ln(\Lambda/T)}{1 + g \ln(\Lambda/T)} + \mathcal{O}(T) \quad (T_c < T \ll \Lambda). \quad (2)$$

The nonuniversal parameters  $c$ ,  $g$ , and  $\Lambda$  are tied to the microscopic properties of the system, with  $\Lambda$  being the lowest relevant energy/frequency scale (we set  $\hbar = k_B = 1$ ), such as  $T_F$ , Debye, or plasma frequency. Negative  $g$  implies the BCS transition at  $T_c = \Lambda e^{-1/|g|}$ , while  $g > 0$  implies its absence, with  $g = 0$  corresponding to QTP. The logarithmic factor in the

numerator—distinguishing (2) from (1)—has the same mathematical origin and, thus, the same expression as the “Tolmachev’s logarithm” in the denominator. However, the two logarithms describe distinctively different physics. The one in the numerator is the pair susceptibility of an *ideal* Fermi liquid (a system with no coupling in the Cooper channel), while the one in the denominator is responsible for Tolmachev’s renormalization of the effective interaction [17,18]. A sharp difference between the stable and unstable regimes develops only at  $|g| \ln(\Lambda/T) > 1$ ; otherwise, susceptibility increases in both regimes regardless of interactions. In the former case,  $\chi_0$  saturates to  $c/g$  at temperatures  $T \ll T_* \simeq \Lambda e^{-1/|g|}$ . These pair correlations (diverging as  $g \rightarrow 0$ ) play a crucial role in the scenario of strange metal behavior discussed in Ref. [19].

For a model with weak momentum-independent interaction, the expression (2) is readily obtained by Bethe-Salpeter summation of the Cooper-channel diagrammatic ladder. Far less trivial is our result shedding light on the previous IR observations [14–16] that Eq. (2) also works in the case of a dynamically screened Coulomb interaction with complex momentum and frequency dependence of the effective coupling in the Cooper channel.

In the context of *ab initio* calculations employing the PCF methodology, we introduce an optimized field-theoretical counterpart of the pair susceptibility,  $R_0$ . As opposed to  $\chi_0$ , the flow of  $R_0$  is free of the “confusing” ideal-Fermi-liquid logarithmic numerator and is characterized by only two parameters,

$$R_0(T) = \frac{1}{1 + g' \ln(\Lambda'/T)} + \mathcal{O}(T). \quad (3)$$

[Consistency with (2) implies  $\ln(\Lambda'/\Lambda) = 1/g' - 1/g$ .] This yields an exciting opportunity for precise theoretical and numerical determination of  $T_c$  and QTP from normal state calculations using a minimal number of fitting parameters (see Figs. 1 and 2).

With the precise method at hand, we performed a model study of the two-dimensional (2D) uniform electron gas (UEG) in the regime of weak-to-moderate interactions, which is interesting for its intrinsic (no-phonons) superconductivity driven by the dynamically screened Coulomb interaction [20–24], as opposed to the original Kohn-Luttinger scenario [25]. Our results (see Fig. 3) reveal a series of QTPs associated with ultralow-temperature superconducting instabilities that we can resolve down to  $10^{-100} T_F$ .

## II. FIELD-THEORETICAL ANALYSIS

Without loss of generality, we study the universal  $s$ -wave linear response scaling laws in a  $d$ -dimensional spherically symmetric homogeneous system (other channels and realistic superconductors are discussed in Appendix A). The linear response functions (2) and (3) originate from the two-electron Green’s function with zero incoming momentum and frequency,  $G_{kp}^{(4)} = \langle \mathcal{T} \hat{\psi}_{k\uparrow}^\dagger \hat{\psi}_{-k\downarrow}^\dagger \hat{\psi}_{-p\downarrow} \hat{\psi}_{p\uparrow} \rangle$ , where  $\hat{\psi}/\hat{\psi}^\dagger$  are the electron annihilation/creation operators. We define the shifted momentum-frequency vector as  $k = (\mathbf{k} - \frac{\mathbf{k}}{|\mathbf{k}|} k_F, \omega_n)$ , where  $\omega_n = (2n + 1)\pi T$  is the fermionic Matsubara frequency. Pair susceptibility  $\chi_0$  is then the

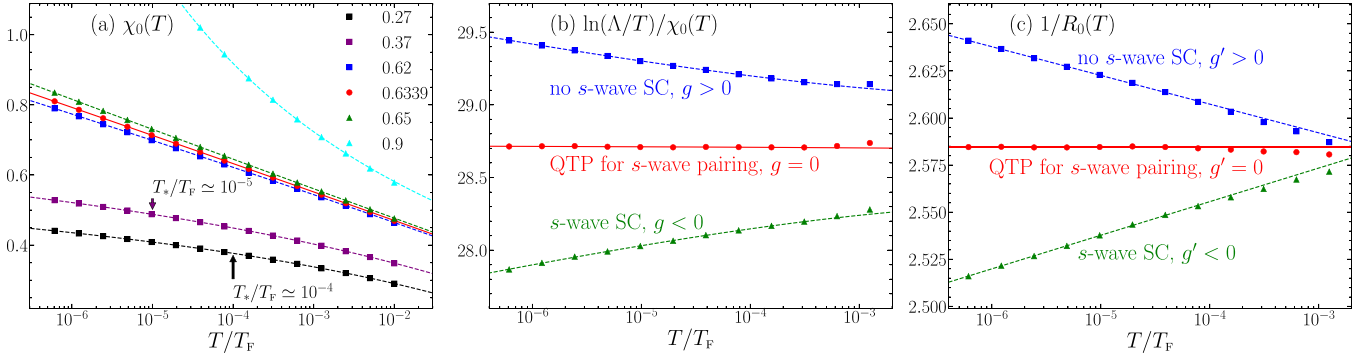


FIG. 2. Temperature evolution of the standard pair susceptibility  $\chi_0$  and modified pair susceptibility  $R_0$  of the 2D uniform electron gas in the  $s$  channel for various values of  $r_s$ . Red circles correspond to QTP  $r_s = 0.6339$ , squares stand for stable regimes ( $g > 0$ ), and triangles are used for the unstable regimes ( $g < 0$ ). The lines are the fits with the ansatz (2) for  $\chi_0$  and ansatz (3) for  $R_0$ . (a) Function  $\chi_0(T)$ . For stable regimes,  $\chi_0(T)$  saturates to a constant at  $T \ll T_* \simeq \Lambda e^{-1/|g|}$ ; for unstable regimes,  $\chi_0(T)$  diverges at  $T = T_c$ ; at the QTP,  $\chi_0(T)$  diverges as  $T \rightarrow 0$ . (b) Inverse  $\chi_0(T)$  rescaled with the ideal-gas logarithmic factor. (c) Inverse  $R_0$ .

linear response to the static uniform pair-field perturbation (of unit amplitude),  $\chi_0 = \int_k \int_p G_{kp}^{(4)}$ , where  $\int_k \equiv T \sum_n \int \frac{d\mathbf{k}}{(2\pi)^d}$ . The momentum-dependent linear response is defined as  $R_k = \int_p G_{kp}^{(4)} / (G_k G_{-k})$ , where  $G_k$  denotes the dressed one-electron Green's function.

We start by analyzing the analytic structure of  $R_k$  as it follows from the self-consistent Bethe-Salpeter equation,

$$R_k = 1 - \int_p \Gamma_{kp} G_p G_{-p} R_p, \quad (4)$$

where  $\Gamma$  is the particle-particle irreducible four-point vertex with zero incoming momentum and frequency. It encodes all effective pairing interactions, such as screened Coulomb potential. The second term on the right-hand side of (4) is a sum of ladder diagrams generated by repeated products of  $\Gamma$  and  $GG$ , each carrying its own set of singularities. The finite-temperature cutoff of  $GG$  at the Fermi surface is responsible for the logarithmic flow that ultimately leads to BCS instability. Concurrently, the vertex function  $\Gamma$  has sin-

gular momentum dependence due to incomplete screening of the long-range Coulomb interaction at any finite frequency. The possible interplay between the two singularities raises the question of whether the flow of the pair susceptibility still follows the same law as in the case of short-range interaction.

The key observation is that Coulomb singularity does not produce large terms when  $\Gamma GG$  is integrated over  $p$ , and the dominant contribution still comes from the BCS logarithm. That is,  $\int_p \Gamma_{kp} G_p G_{-p} = \tilde{g}_k \ln T + \tilde{f}_k + \mathcal{O}(T)$ , where  $\tilde{g}_k$  and  $\tilde{f}_k$  are temperature-independent and regular-in- $k$  functions, and the finite- $T$  corrections vanish at least linearly with  $T$ . Further technical details are provided elsewhere [26]. This observation allows one to parametrize  $\Gamma GG$  as

$$\Gamma_{kp} G_p G_{-p} \rightarrow [\tilde{g}_k \ln T + \tilde{f}_k] \delta_p + \phi_{kp}, \quad (5)$$

where  $\delta_p = \frac{(2\pi)^d \Gamma(\frac{d}{2})}{4\pi^{d/2} T} \delta(|\omega_m| - \pi T) \delta(|\mathbf{p}| - k_F)$  (as expected,  $\int_p \delta_p = 1$ ), and the regular correction satisfies  $\int_p \phi_{kp} = \mathcal{O}(T)$ . By incorporating this form into Eq. (4), we obtain the temperature dependence of the linear response,

$$R_k = \frac{1 + (f_k - f_0) + (g_k - g_0) \ln T}{1 - f_0 - g_0 \ln T} + \mathcal{O}(T), \quad (6)$$

where  $f_k$  and  $g_k$  are regular functions representing  $\tilde{f}_k$  and  $\tilde{g}_k$  renormalized by pair fluctuations. Remarkably, the logarithmic correction in the numerator vanishes in the low-energy limit  $k \rightarrow 0$ , resulting in a simple relation for  $R_0 \equiv R_{k \rightarrow 0}$  given by Eq. (3) with  $g' = g_0$  and  $\Lambda' = e^{-f_0/g_0}$ . The pair susceptibility  $\chi_0 = \int_k R_k G_k G_{-k}$ , on the other hand, involves  $R_k$  with finite  $k$  and, thus, retains the global logarithmic factor.

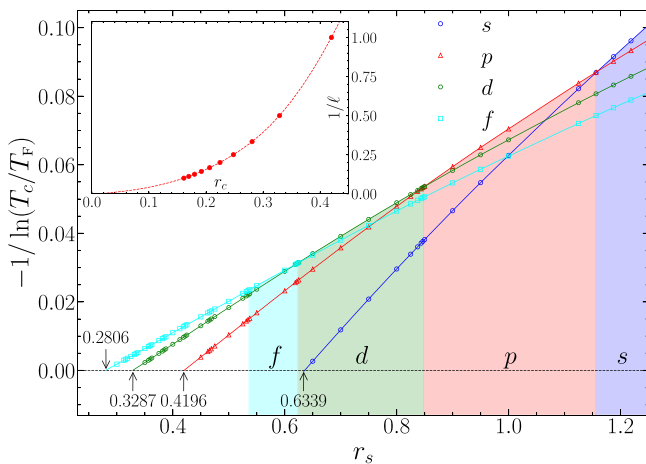


FIG. 3. Superconducting phase diagram of the 2D UEG. For each channel, the line starting at QTP shows the (would-be) critical temperature. Critical values of  $r_s$  for  $\ell$  as large as 10 are presented in the inset.

### III. SUPERCONDUCTIVITY IN THE 2D UNIFORM ELECTRON GAS

In the absence of electron-phonon interaction, superconductivity in this model is of the emergent BCS type, and the values of  $T_c$  are supposed to be extremely low. The theory presented above and advanced numerical techniques not only allow us to study many pairing channels, but also accurately locate QTP when  $T_c$  goes to zero.

Previous studies [15,22] revealed the existence of high-orbital-momentum  $\ell$  superconducting states in the 3D UEG in the weak-coupling limit when the random phase approximation (RPA) becomes controllably accurate. The pairing comes from dynamic nature screening in Coulomb systems, as discussed by Rieschel and Sham [20,27], and not from the static Kohn-Luttinger mechanism [25]. In light of the pioneering work by Takada [21], we expect that the dynamic character of screening will play a crucial role in 2D as well.

In the weak-coupling limit, the RPA vertex function  $\Gamma$  has the form

$$\Gamma_{\mathbf{p},\omega_m}^{\mathbf{k},\omega_n} \approx \frac{V_{\mathbf{p}-\mathbf{k}}}{1 + V_{\mathbf{p}-\mathbf{k}} \cdot \Pi_0(\mathbf{p} - \mathbf{k}, \omega_m - \omega_n)}, \quad (7)$$

where  $V_{\mathbf{q}} = 2\pi e^2/q$  is the bare Coulomb repulsion and  $\Pi_0(\mathbf{p} - \mathbf{k}, \omega_m - \omega_n)$  is the RPA polarization. At this level of accuracy, we consider bare Green's functions  $G_{\mathbf{k},\omega_n} = 1/(i\omega_n - \mathbf{k}^2/2m + E_F)$  in Eq. (4), where  $m$  is the electron mass [Fermi temperature can be expressed as  $T_F = 1/(ma_B^2 r_s^2)$ , where  $r_s = \sqrt{2}/(k_F a_B)$  with the Bohr radius  $a_B$ ].

To efficiently solve Eq. (4) at ultralow temperatures, we employ the discrete Lehmann representation (DLR) [16,28,29] to radically reduce the computational cost of representing the linear response and Green's functions from  $\mathcal{O}(1/T\epsilon)$  for uniform grids to  $\mathcal{O}[\ln(1/T)\ln(1/\epsilon)]$ , where  $\epsilon$  is the error tolerance. The codes are available online [30].

We performed systematic calculations of  $R_0$  for various orbital channels  $\ell$  and values of  $r_s$ . For each  $\ell$  and  $r_s$ , we determine the transition temperature by extrapolating  $1/R_0(T)$  flows to zero using the least-squares criterion. Subsequently, for each  $\ell$ , we extrapolate results for  $-1/\ln[T_c(r_s)/T_F]$  to zero to reveal critical values of  $r_s$ . The phase diagram of competing superconducting states in the 2D UEG is shown in Fig. 3.

As expected, by increasing density (decreasing  $r_s$ ), one suppresses  $T_c$  in all orbital channels. While all channels are superconducting at  $r_s \sim 1$ , they successively go through QTPs so that only large  $\ell$  channels stay superconducting at small  $r_s$ . Accordingly, the orbital index of the dominant (highest- $T_c$ ) channel also increases with density [we obtain it from crossing points between the  $T_c^{(\ell)}(r_s)$  and  $T_c^{(\ell+1)}(r_s)$  curves]. The smooth dependence of  $-1/\ln(T_c/T_F)$  on  $r_s$  leads to the accurate determination of the QTP by linear extrapolation. We observe that  $-1/\ln[T_c^{(\ell)}/T_F] \approx (r_s - r_c^{(\ell)})/c_\ell$ , where  $c_\ell$  is a dimensionless constant, i.e., in the vicinity of QTP, the transition temperature obeys  $T_c^{(\ell)} = T_F e^{-1/c_\ell}$  [31,32], with  $\lambda_\ell = (r_s - r_c^{(\ell)})/c_\ell$ .

Data in the inset in Fig. 3 suggest that superconductivity in the 2D UEG survives in the high-density limit ( $r_s \rightarrow 0$ ) for large enough  $\ell$ . We emphasize that this outcome cannot be explained by the Kohn-Luttinger mechanism because, in 2D, this mechanism simply does not exist at the RPA level [33]. Similar to the 3D case, we are dealing with the consequences of dynamic screening in systems with long-range interactions. To explore how the interaction range changes the picture, we took density corresponding to  $r_s = 0.8$  (when all channels are superconducting) and replaced the Coulomb potential with the Yukawa one. We find that for screening length  $\sim 1/k_F$ , all of the channels mentioned in Fig. 3 are no longer superconducting. For more details, see the Appendix.

Finally, we recalculated the phase diagram by accounting for renormalization of the Green's function within the  $G_0W_0$  approximation for the proper self-energy. Qualitative (and quantitative at small  $r_s$ ) agreement between the phase diagrams presented in the Appendix and Fig. 3 demonstrates the robustness of our conclusions.

#### IV. CONCLUSIONS AND OUTLOOK

We have shown that pair susceptibility (linear response to a static spatially uniform pair-creating perturbation) of the normal Fermi liquid features is universal for all BCS superconductors' temperature dependence, or "flow," given by Eq. (2), irrespective of the emergent pairing mechanism. The ansatz (2) applies to both stable and unstable pairing channels. In both cases, the higher-temperature part of the flow is the same, up to small corrections, and represents a response that is singular in the  $T \rightarrow 0$  limit of an ideal Fermi liquid. A sharp difference between the stable and unstable cases develops only at exponentially low temperatures: the unstable channel hits finite-temperature singularity at  $T_c$ , while the stable channel develops nontrivial correlations suppressing the zero-temperature singularity. The  $T = 0$  singularity survives only at the quantum transition points (QTPs) separating the stable and unstable regimes.

Using two-dimensional uniform electron gas as a paradigmatic model of intrinsic superconductivity mediated by dynamic screening of Coulomb interaction, we demonstrated that fitting the normal Fermi liquid data to the ansatz (2)—and its numeric counterpart (3)—allows one to accurately predict ultralow critical temperatures of unstable Cooper channels and locate QTPs.

We anticipate that our method for controlled quantitative predictions of ultralow-temperature Cooper instability (or its absence) from finite-temperature flows of the linear response to a spatially uniform pair-creating perturbation can be extended to cases where the perturbation is applied at the boundaries of the normal state. This would be the theoretical basis for experimental studies of precursory Cooper flows in the normal metallic state by using superconductor–normal metal–superconductor tunnel junction setups [8–13] in the high-temperature range  $T_c \ll T \ll T_F$ . For metals such as Cu, Au, and Na, where superconductivity at ultralow temperature remains uncertain, it would be equally informative to observe whether flows (2) correspond to negative or positive values of  $g$  in the  $s$  channel.

#### ACKNOWLEDGMENTS

We thank A. Chubukov for valuable discussions. P.H. and Y.D. were supported by the National Natural Science Foundation of China (Grant No. 12275263), the Innovation Program for Quantum Science and Technology (Grant No. 2021ZD0301900), and the National Key R&D Program of China (Grant No. 2018YFA0306501). N.P., B.S., and T.W. were supported by the National Science Foundation under Grant No. DMR-2032077. X.C. and K.C. were supported by the Simons Collaboration on the Many Electron Problem. The Flatiron Institute is a division of the Simons Foundation. K.C. is supported by Project No. 12047503 of National Natural Science Foundation of China.

## APPENDIX A: ANGULAR MOMENTUM DECOMPOSITION IN TWO AND HIGHER DIMENSIONS

In an isotropic system, the particle-particle four-point vertex with zero incoming momentum and frequency,  $\Gamma_{\mathbf{p},\omega_m}^{\mathbf{k},\omega_n}$ , only depends on the angle between  $\mathbf{k}$  and  $\mathbf{p}$  ( $\theta_{\hat{k}p} \equiv \theta_k - \theta_{\hat{p}}$ ), their moduli, and the Matsubara-frequencies difference  $\omega_n - \omega_m$ . This allows us to simplify the analysis by projecting  $\Gamma$  onto different orbital channels  $\ell$ . In this Appendix, the frequency variables and Matsubara summation are omitted for brevity as they do not affect the decomposition.

Considering the Bethe-Salpeter equation for the linear response function  $R$ ,

$$R_{\mathbf{k}} = \eta_{\mathbf{k}} - \int \frac{d\mathbf{p}}{(2\pi)^d} \Gamma_{\mathbf{p}}^{\mathbf{k}} F_{\mathbf{p}}, \quad (\text{A1})$$

where  $\eta_{\mathbf{k}}$  is the sourced term and  $F_{\mathbf{p}} = G_{\mathbf{p}} G_{-\mathbf{p}} R_{\mathbf{p}}$ , we can project it onto decoupled orbital channels  $\ell$  via an expansion. After the projection to the angular momentum sector,  $R$  and  $\Gamma$  are solely dependent on the momentum amplitudes, allowing a unified treatment of generic dimension.

In two dimensions, the vertex function can be expressed as a Fourier expansion,

$$\begin{aligned} \Gamma_{|\mathbf{k}-\mathbf{p}|} &= \frac{\Gamma^{(0)}}{2\pi} + \sum_{\ell=1}^{\infty} \Gamma_{k,p}^{(\ell)} \frac{\cos \ell \theta_{\hat{k}p}}{\pi}, \\ \Gamma_{k,p}^{(\ell)} &= \int_0^{2\pi} d\theta_{\hat{k}p} \Gamma(\sqrt{k^2 + p^2 - 2kp \cos \theta_{\hat{k}p}}) \cos \ell \theta_{\hat{k}p}. \end{aligned} \quad (\text{A2})$$

Apart from the  $\Gamma$  expansion, given by Eq. (A2), we also need to expand functions that depend only on one momentum variable,

$$O_{\mathbf{k}} = \frac{O_k^{(0)}}{2\pi} + \sum_{\ell=1}^{\infty} O_k^{(\ell)} \frac{\cos \ell \theta_{\hat{k}}}{\pi} + \overline{O}_k^{(\ell)} \frac{\sin \ell \theta_{\hat{k}}}{\pi}, \quad (\text{A3})$$

where  $O$  represents  $R$ ,  $F$ , or  $\eta$ ,  $O_k^{(\ell)} = \int_0^{2\pi} d\theta_{\hat{k}} \cos \ell \theta_{\hat{k}} O_{\mathbf{k}}$ , and  $\overline{O}_k^{(\ell)} = \int_0^{2\pi} d\theta_{\hat{k}} \sin \ell \theta_{\hat{k}} O_{\mathbf{k}}$ . The convolution term in Eq. (A1) can also be expanded in Fourier series,

$$\begin{aligned} &\int \frac{d\mathbf{p}}{(2\pi)^2} \Gamma_{|\mathbf{k}-\mathbf{p}|} F_{\mathbf{p}} \\ &= \int \frac{d\mathbf{p}}{(2\pi)^2} \left[ \left( \frac{\Gamma_{k,p}^{(0)}}{2\pi} + \sum_{\ell=1}^{\infty} \Gamma_{k,p}^{(\ell)} \frac{\cos \ell \theta_{\hat{k}p}}{\pi} \right) \left( \frac{F_p^{(0)}}{2\pi} + \sum_{\ell'=1}^{\infty} F_p^{(\ell')} \frac{\cos \ell' \theta_{\hat{p}}}{\pi} + \overline{F}_p^{(\ell')} \frac{\sin \ell' \theta_{\hat{p}}}{\pi} \right) \right] \\ &= \int \frac{pd p}{(2\pi)^2} \left\{ \Gamma_{k,p}^{(0)} \frac{F_p^{(0)}}{2\pi} + \sum_{\ell=1}^{\infty} \Gamma_{k,p}^{(\ell)} \int_0^{2\pi} \frac{d\theta_{\hat{p}}}{\pi} (\cos \ell \theta_{\hat{k}} \cos \ell \theta_{\hat{p}} + \sin \ell \theta_{\hat{k}} \sin \ell \theta_{\hat{p}}) \sum_{\ell'=1}^{\infty} \left[ F_p^{(\ell')} \frac{\cos \ell' \theta_{\hat{p}}}{\pi} + \overline{F}_p^{(\ell')} \frac{\sin \ell' \theta_{\hat{p}}}{\pi} \right] \right\} \\ &= \int \frac{pd p}{(2\pi)^2} \left[ \Gamma_{k,p}^{(0)} \frac{F_p^{(0)}}{2\pi} + \sum_{\ell=1}^{\infty} \Gamma_{k,p}^{(\ell)} \left( F_p^{(\ell)} \frac{\cos \ell \theta_{\hat{k}}}{\pi} + \overline{F}_p^{(\ell)} \frac{\sin \ell \theta_{\hat{k}}}{\pi} \right) \right], \end{aligned} \quad (\text{A4})$$

where  $F_p^{(\ell)} = G_p G_{-p} R_p^{(\ell)}$  and  $R_p^{(\ell)} = \int_0^{2\pi} d\theta_{\hat{p}} \cos \ell \theta_{\hat{p}} R_{\mathbf{p}}$  (the product of two Green's functions is isotropic). Therefore, the linear response function for each channel is given by

$$R_k^{(\ell)} = 1 - \int \frac{pd p}{(2\pi)^2} \Gamma_{k,p}^{(\ell)} G_p G_{-p} R_p^{(\ell)}. \quad (\text{A5})$$

Here, by setting  $\eta^{(\ell)} \equiv 1$  and projecting into channel  $\ell$ , we break the U(1) symmetry and the rotation symmetry so that the result for different channels can be obtained separately.

In three or higher dimensions, the angular momentum decomposition can be achieved by a similar approach using expansion in the spherical harmonics. The vertex function can be expressed as an expansion in Legendre polynomials  $P_{\ell}(x)$ ,

$$\begin{aligned} \Gamma_{|\mathbf{k}-\mathbf{p}|} &= \sum_{\ell=0}^{\infty} \frac{N(d, \ell)}{2} \Gamma_{k,p}^{(\ell)} P_{\ell}(x), \\ \Gamma_{k,p}^{(\ell)} &= \int_{-1}^1 dx \Gamma(\sqrt{k^2 + p^2 - 2kp x}) P_{\ell}(x), \end{aligned} \quad (\text{A6})$$

where  $x = \cos \theta_{\hat{k}p}$  and  $N(d, \ell) = \frac{2\ell+d-2}{\ell} \binom{\ell+d-3}{\ell-1}$  denotes the number of linearly independent Legendre polynomials of degree  $\ell$  in  $d$  dimensions. Using the addition theorem for

spherical harmonics [34],

$$P_{\ell}(x) = \frac{\Omega_d}{N(d, \ell)} \sum_{m=1}^{N(d, \ell)} Y_{\ell m}(\theta_{\hat{k}}) Y_{\ell m}^*(\theta_{\hat{p}}), \quad (\text{A7})$$

where  $\Omega_d = (2\pi)^{\frac{d}{2}}/\Gamma(d/2)$  is the solid angle in  $d$  dimensions and  $Y_{\ell m}(\theta)$  is the spherical harmonic function, the vertex function can be expressed further on as

$$\Gamma_{|\mathbf{k}-\mathbf{p}|} = \frac{\Omega_d}{2} \sum_{\ell=0}^{\infty} \Gamma_{k,p}^{(\ell)} Y_{\ell 0}(\theta_{\hat{k}}) Y_{\ell 0}^*(\theta_{\hat{p}}). \quad (\text{A8})$$

Here we set  $m = 0$  because the decomposed equation is independent of  $m$  for a system with rotation symmetry. The linear response function can also be decomposed as

$$R_{\mathbf{k}} = \sum_{\ell=0}^{\infty} R_k^{(\ell)} Y_{\ell 0}(\theta_{\hat{k}}), \quad (\text{A9})$$

where  $R_k^{(\ell)} = \int d\theta_{\hat{k}} R_{\mathbf{k}} Y_{\ell 0}(\theta_{\hat{k}})$ . Projecting the convolution term in Eq. (A1) on the spherical harmonics,

we obtain

$$\begin{aligned}
& \int \frac{d\mathbf{p}}{(2\pi)^d} \Gamma_{|\mathbf{k}-\mathbf{p}|} F_{\mathbf{p}} \\
&= \frac{\Omega_d}{2} \int \frac{d\mathbf{p}}{(2\pi)^d} G_p G_{-p} \\
&\times \sum_{\ell=0}^{\infty} \Gamma_{k,p}^{(\ell)} Y_{\ell 0}(\theta_{\hat{k}}) Y_{\ell 0}^*(\theta_{\hat{p}}) \sum_{\ell'=0}^{\infty} R_k^{(\ell')} Y_{\ell' 0}(\theta_{\hat{k}}) \\
&= \sum_{\ell=0}^{\infty} \frac{\Omega_d}{2} \int \frac{p^{d-1} dp}{(2\pi)^d} \Gamma_{k,p}^{(\ell)} R_k^{(\ell)} Y_{\ell 0}(\theta_{\hat{k}}), \quad (\text{A10})
\end{aligned}$$

where the orthonormal property of the spherical harmonics as  $\int d\theta_{\hat{k}} Y_{\ell m}(\theta_{\hat{k}}) Y_{\ell' m'}^*(\theta_{\hat{k}}) = \delta_{\ell\ell'} \delta_{mm'}$  is utilized.

Finally, we have the decoupled self-consistent linear response equation for each orbital channel in  $d$  ( $\geq 3$ ) dimensions as

$$R_k^{(\ell)} = 1 - \frac{\Omega_d}{2} \int \frac{p^{d-1} dp}{(2\pi)^d} \Gamma_{k,p}^{(\ell)} G_p G_{-p} R_p^{(\ell)}, \quad (\text{A11})$$

where only the measure of momentum integral is different from two dimensions. We can unify both Eq. (A5) and Eq. (A11) with the following simplified expression:

$$R_K = 1 - \int dP \Gamma_{K,P} G_P^{(2)} R_P, \quad (\text{A12})$$

where we introduce the momentum-frequency variable  $P = (\Delta p, \omega_m)$  with  $\Delta p = p - k_F$  and  $G_P^{(2)} \equiv G_P G_{-P}$ . The integral is defined as  $\int dP \equiv T \sum_m \int d\Delta p$ . We have also defined  $\Gamma_{K,P} = \frac{p}{4\pi^2} \Gamma_{k,p}^{(\ell)}$  in two dimensions and  $\frac{p^{d-1} \Omega_d}{2(2\pi)^d} \Gamma_{k,p}^{(\ell)}$  in higher dimensions to absorb the measure of momentum integral. The  $\ell$  label in  $R_k^{(\ell)}$  is omitted.

## APPENDIX B: SUPERCONDUCTING PHASES OF THE TWO-DIMENSIONAL ELECTRON GAS WITH $G_0 W_0$ SELF-ENERGY RENORMALIZATION

We employed the precursory Cooper flow approach to investigate dynamic-screening-driven superconductivity in the two-dimensional uniform electron gas (2D UEG) model, parametrized by the Wigner-Seitz radius  $r_s = \sqrt{2}/(k_F a_B)$ , where  $k_F$  is the Fermi momentum and  $a_B$  is the Bohr radius. As shown in Fig. 1, we obtained a rich phase diagram for several channels.

To verify the robustness of the pairing mechanism in the 2D UEG, here we computed the same phase diagram using the RPA interaction for  $\Gamma$  and the  $G_0 W_0$  renormalized propagator  $G^R$  (referred to as RPA- $G^R$ ), as shown in Fig. 4. A comparison with the RPA- $G_0$  results presented in the main text reveals small shifts of the phase boundaries, but all key features of the RPA- $G_0$  phase diagrams are preserved for RPA- $G^R$ , as follows: (i) The critical temperature  $T_c$  in all orbital channels is suppressed as the density increases ( $r_s$  decreases) and eventually becomes zero at the quantum transition point (QTP)  $r_c^{(\ell)}$ , below which the 2D UEG no longer superconducts. (ii) On the logarithmic scale,  $-1/\ln[T_c(r_s)/T_F]$  still demonstrates a linear dependence on  $r_s$  near the QTP, indicating that the BCS transition temperature obeys  $T_c^{(\ell)} = T_F e^{-1/\lambda_\ell}$  with the coupling parameter  $\lambda_\ell = (r_s - r_c^{(\ell)})/c_\ell$ , where  $c_\ell$  is a constant.

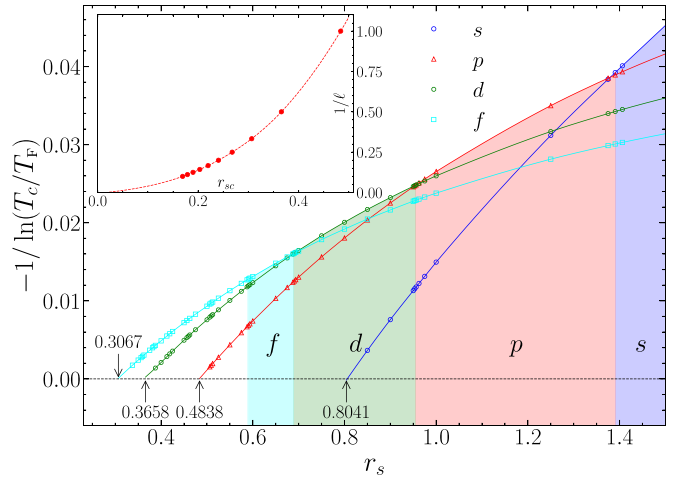


FIG. 4. Phase diagram of superconducting states in the 2D UEG within the RPA- $G^R$  framework showing  $s$ -,  $p$ -,  $d$ -, and  $f$ -wave superconducting states. Each orbital channel features a QTP with  $T_c^{(\ell)}(r_s \rightarrow r_c^{(\ell)}) \rightarrow 0$ . Critical values of  $r_s$  for  $\ell$  as large as 10 are presented in the inset.

(iii) The data for  $1/\ell$  versus  $r_c$  in the inset of Fig. 4 suggest that superconductivity survives in the high-density limit for large enough  $\ell$ . The qualitative agreement between the RPA- $G_0$  and RPA- $G^R$  phase diagrams reflects the robustness of dynamic-screening-driven superconductivity in the 2D UEG.

## APPENDIX C: SUPERCONDUCTING PHASES OF THE TWO-DIMENSIONAL ELECTRON GAS WITH YUKAWA-TYPE INTERACTION

To investigate the impact of interaction range on the dynamic-screening-driven superconductivity in two dimensions, we consider the 2D electron gas with the Yukawa-type interaction  $V_Y(q) = 2\pi e^2 / \sqrt{q^2 + q_0^2}$ , also known as a statically screened Coulomb interaction, where  $q_0$  is the screening momentum. Specifically, we examine the behavior of the superconducting state in the 2D electron gas at  $r_s = 0.8$  when all channels exhibit superconductivity in the Coulomb system. We performed systematic and extensive calculations of the linear response function  $R$  for various channels  $\ell$  and values of  $q_0$  using RPA- $G_0$  and RPA- $G^R$ , respectively.

For each  $\ell$  and  $q_0$ , we determined the transition temperature  $T_c$  by extrapolating the precursory Cooper flow to  $1/R_0(T_c) = 0$ . Subsequently, we used extrapolation to determine the critical values of  $q_0$  ( $q_{0c}$ ), where  $-1/\ln[T_c(q_0)/T_F]$  becomes zero and superconductivity vanishes. Finally, we obtained the phase diagrams in the 2D electron gas with the Yukawa-type interaction under the RPA- $G_0$  [Fig. 5(a)] and RPA- $G^R$  [Fig. 5(b)] approximations, respectively. The qualitative agreement between the two phase diagrams indicates that the approximations are controlled.

As the range of interaction decreases (i.e., as  $q_0$  increases), the superconducting critical temperature  $T_c$  decreases for any given channel  $\ell$  and eventually drops to zero at the QTP with the critical screening momentum  $q_{0c}^{(\ell)}$ . Since the rate of the  $T_c$  drop slows as  $\ell$  increases, the dominant superconducting channel, determined from the crossing point of  $T_c^{(\ell)}(q_0)$

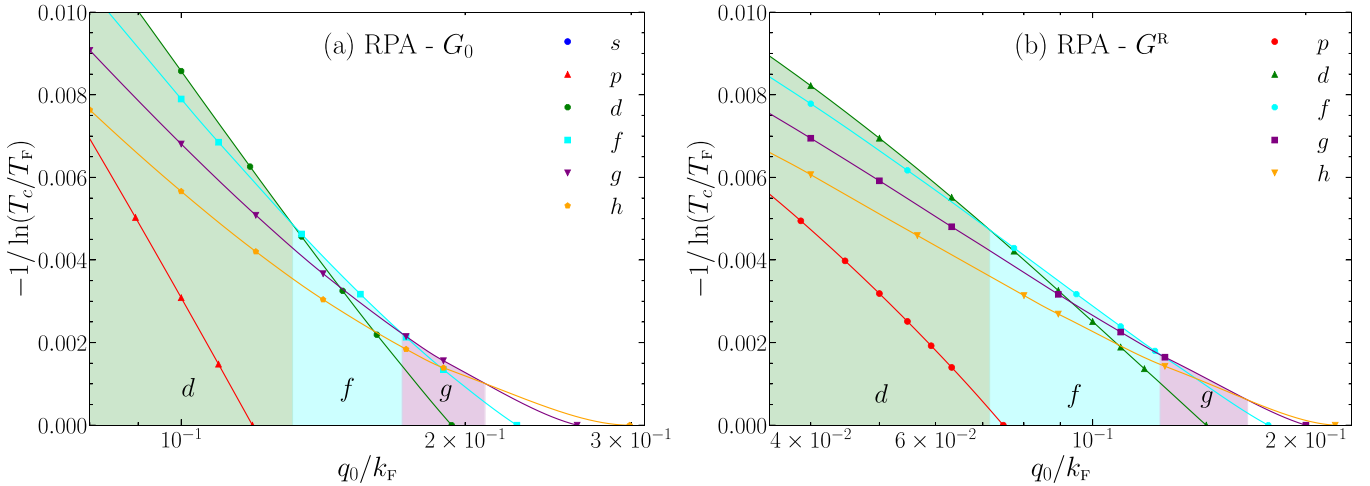


FIG. 5. Ultralow-temperature phase diagram of a 2D electron gas with  $r_s = 0.8$  and a Yukawa-type interaction  $V_Y(q) = 2\pi e^2 / \sqrt{q^2 + q_0^2}$ , calculated using the (a) RPA- $G_0$  and (b) RPA- $G^R$  approximations. The superconducting temperature ( $T_c$ ) as a function of the screening momentum ( $q_0$ ) is represented by lines going through data points for different channels, with the colored shadow indicating the dominant channel. For any given channel  $\ell$ ,  $T_c^{(\ell)}$  decreases with increasing  $q_0$  until it disappears at the critical value  $q_{0c}^{(\ell)}$ .

and  $T_c^{(\ell+1)}(q_0)$ , increases as  $q_0$  increases. Surprisingly, for  $q_0 > 0.2k_F$ , all of the orbital channels shown in Fig. 5 are no longer superconducting. These observations suggest that the long-range character of the Coulomb interaction is essential in dynamic-screening-driven superconductivity and that decreasing the interaction range suppresses superconductivity in the 2D electron gas. Furthermore, for  $q_0 \rightarrow q_{0c}^-$ , a linear relation exists between the inverse logarithmic scale  $-1/\ln[T_c(q_0)/T_F]$  and  $q_0$ , indicating that the superconductivity near the QTP can be described by the emergent BCS theory with a coupling parameter  $\lambda'_\ell \propto (q_{0c} - q_0)/k_F \ll 1$ .

TABLE I. The critical  $r_s$  parameters for the 2D electron gas under the RPA- $G_0$  and RPA- $G^R$  approximations for various orbital channels  $\ell$ . In this table,  $r_c^{\text{RPA-}G_0}$  and  $r_c^{\text{RPA-}G^R}$  denote the critical  $r_s$  values for the disappearance of superconductivity in each channel under RPA- $G_0$  and RPA- $G^R$  approximations, respectively. Meanwhile,  $r_{st}^{\text{RPA-}G_0}(\ell \rightarrow \ell + 1)$  and  $r_{st}^{\text{RPA-}G^R}$  represent the critical  $r_s$  values for the transition from channel  $\ell$  to  $\ell + 1$  under the respective approximations.

$\ell$	$r_c^{\text{RPA-}G_0}$	$r_c^{\text{RPA-}G^R}$	$r_{st}^{\text{RPA-}G_0}(\ell \rightarrow \ell + 1)$	$r_{st}^{\text{RPA-}G^R}$
0	0.6339(12)	0.8041(25)	1.156(3)	1.391(16)
1	0.4196(10)	0.4838(20)	0.8484(16)	0.9547(16)
2	0.3287(10)	0.3658(17)	0.6234(16)	0.6891(16)
3	0.2806(10)	0.3067(11)	0.5359(16)	0.5891(16)
4	0.2479(6)	0.2678(11)	0.4672(16)	0.5078(16)
5	0.2244(7)	0.2405(18)	0.4234(16)	0.4578(16)
6	0.2062(5)	0.2198(20)	0.3859(16)	0.416(3)
7	0.1918(8)	0.2033(10)	0.3578(16)	0.3828(16)
8	0.1798(5)	0.1898(10)	0.3359(16)	0.3578(16)
9	0.1698(4)	0.1787(10)	0.3141(16)	0.331(6)
10	0.1611(5)	0.1692(14)		

#### APPENDIX D: DATA TABLE OF QUANTUM TRANSITION POINTS

The results for quantum transition points  $r_c^{(\ell)}$  and left boundaries of the dominant superconducting channel  $r_{st}(\ell \rightarrow \ell + 1)$  for various orbital channels  $\ell$  are given in Table I. The data for dimensionless critical screening momentum  $q_{0c}^{(\ell)}$  at  $r_s = 0.8$  are given in Table II.

TABLE II. Critical screening momentum  $q_{0c}$  (in units of the Fermi momentum  $k_F$ ) of the 2D electron gas with a Yukawa-type interaction under the RPA- $G_0$  and RPA- $G^R$  approximations at  $r_s = 0.4$  and 0.8. Note that  $s$ -wave superconductivity is absent in the 2D electron gas with RPA- $G^R$  at  $r_s = 0.8$  and  $q_0 = 0$ .

$r_s$	$\ell$	$q_{0c}^{\text{RPA-}G_0}$	$q_{0c}^{\text{RPA-}G^R}$
0.4	2	0.00674(15)	0.00152(7)
	3	0.0193(2)	0.0110(3)
	4	0.0313(3)	0.0216(5)
	5	0.0409(4)	0.0306(7)
	6	0.0490(5)	0.0382(8)
	7	0.0557(6)	0.0445(9)
	8	0.0615(6)	0.0500(10)
	9	0.0666(6)	0.0546(11)
	10	0.0713(7)	0.0588(13)
	0	0.0205(5)	
0.8	1	0.1190(11)	0.0748(7)
	2	0.1936(13)	0.1446(18)
	3	0.2270(11)	0.177(6)
	4	0.263(4)	0.205(5)
	5	0.299(7)	0.228(9)

**APPENDIX E: DATA TABLE OF SUPERCONDUCTING TEMPERATURES  
OF THE TWO-DIMENSIONAL ELECTRON GAS**

All of the superconducting transition temperature  $T_c^{(\ell)}$  data are given in Table III with RPA- $G_0$  and Table IV with RPA- $G^R$ .

TABLE III. Superconducting temperatures  $T_c^{(\ell)}$  (in units of the Fermi temperature  $T_F$ ) for different  $r_s$  from RPA- $G_0$ . The “–” symbol means that the  $T_c$  value is lower than the limit of double-precision floating-point number resolution.

$r_s$	$T_c^{(0)}$	$T_c^{(1)}$	$T_c^{(2)}$	$T_c^{(3)}$
0.300000	0	0	0	$1.406 \times 10^{-237}$
0.312500	0	0	0	$4.072 \times 10^{-147}$
0.315625	0	0	0	$2.579 \times 10^{-134}$
0.318750	0	0	0	$1.469 \times 10^{-123}$
0.325000	0	0	0	$1.695 \times 10^{-106}$
0.331250	0	0		$1.4249 \times 10^{-93}$
0.334375	0	0		$3.2153 \times 10^{-88}$
0.337500	0	0		$1.9099 \times 10^{-83}$
0.350000	0	0	$1.280 \times 10^{-189}$	$1.3299 \times 10^{-68}$
0.356250	0	0	$2.575 \times 10^{-147}$	$5.2761 \times 10^{-63}$
0.359375	0	0	$1.572 \times 10^{-132}$	$1.5520 \times 10^{-60}$
0.362500	0	0	$1.927 \times 10^{-120}$	$2.9667 \times 10^{-58}$
0.375000	0	0	$2.9758 \times 10^{-88}$	$1.2427 \times 10^{-50}$
0.381250	0	0	$7.3936 \times 10^{-78}$	$1.5765 \times 10^{-47}$
0.384375	0	0	$1.5728 \times 10^{-73}$	$4.0684 \times 10^{-46}$
0.387500	0	0	$1.1665 \times 10^{-69}$	$8.6837 \times 10^{-45}$
0.400000	0	0	$1.4701 \times 10^{-57}$	$3.6303 \times 10^{-40}$
0.412500	0	0	$4.6208 \times 10^{-49}$	$2.0135 \times 10^{-36}$
0.418750	0	0	$1.0688 \times 10^{-45}$	$8.3380 \times 10^{-35}$
0.421875	0		$3.4799 \times 10^{-44}$	$4.7395 \times 10^{-34}$
0.425000	0		$9.0343 \times 10^{-43}$	$2.4979 \times 10^{-33}$
0.450000	0	$2.007 \times 10^{-112}$	$4.3625 \times 10^{-34}$	$1.6146 \times 10^{-28}$
0.462500	0	$1.2949 \times 10^{-79}$	$5.7451 \times 10^{-31}$	$1.2998 \times 10^{-26}$
0.465625	0	$3.2625 \times 10^{-74}$	$2.8157 \times 10^{-30}$	$3.5458 \times 10^{-26}$
0.468750	0	$1.6743 \times 10^{-69}$	$1.2848 \times 10^{-29}$	$9.3524 \times 10^{-26}$
0.475000	0	$1.0989 \times 10^{-61}$	$2.1986 \times 10^{-28}$	$5.9198 \times 10^{-25}$
0.500000	0	$1.4072 \times 10^{-42}$	$2.0830 \times 10^{-24}$	$2.8734 \times 10^{-22}$
0.525000	0	$1.1742 \times 10^{-32}$	$2.2786 \times 10^{-21}$	$4.9251 \times 10^{-20}$
0.531250	0	$7.2448 \times 10^{-31}$	$9.7356 \times 10^{-21}$	$1.4711 \times 10^{-19}$
0.534375	0	$4.8022 \times 10^{-30}$	$1.9460 \times 10^{-20}$	$2.4908 \times 10^{-19}$
0.537500	0	$2.8769 \times 10^{-29}$	$3.8086 \times 10^{-20}$	$4.1629 \times 10^{-19}$
0.550000	0	$1.5595 \times 10^{-26}$	$4.6101 \times 10^{-19}$	$2.8777 \times 10^{-18}$
0.600000	0	$2.0370 \times 10^{-19}$	$9.6175 \times 10^{-16}$	$1.4137 \times 10^{-15}$
0.618750	0	$1.1135 \times 10^{-17}$	$8.4689 \times 10^{-15}$	$8.9310 \times 10^{-15}$
0.621875	0	$2.0163 \times 10^{-17}$	$1.1839 \times 10^{-14}$	$1.1902 \times 10^{-14}$
0.625000	0	$3.5848 \times 10^{-17}$	$1.6431 \times 10^{-14}$	$1.5776 \times 10^{-14}$
0.650000	$6.976 \times 10^{-162}$	$2.0240 \times 10^{-15}$	$1.7896 \times 10^{-13}$	$1.2623 \times 10^{-13}$
0.700000	$2.0992 \times 10^{-37}$	$7.2375 \times 10^{-13}$	$7.9388 \times 10^{-12}$	$3.7862 \times 10^{-12}$
0.750000	$1.3675 \times 10^{-21}$	$4.2496 \times 10^{-11}$	$1.4054 \times 10^{-10}$	$5.4233 \times 10^{-11}$
0.800000	$2.1308 \times 10^{-15}$	$8.3996 \times 10^{-10}$	$1.3343 \times 10^{-09}$	$4.6029 \times 10^{-10}$
0.825000	$1.5734 \times 10^{-13}$	$2.8191 \times 10^{-09}$	$3.4548 \times 10^{-09}$	$1.1534 \times 10^{-09}$
0.837500	$9.0592 \times 10^{-13}$	$4.8863 \times 10^{-09}$	$5.3631 \times 10^{-09}$	$1.7689 \times 10^{-09}$
0.843750	$2.0085 \times 10^{-12}$	$6.3537 \times 10^{-09}$	$6.6275 \times 10^{-09}$	$2.1747 \times 10^{-09}$
0.846875	$2.9382 \times 10^{-12}$	$7.2240 \times 10^{-09}$	$7.3530 \times 10^{-09}$	$2.4070 \times 10^{-09}$
0.850000	$4.2506 \times 10^{-12}$	$8.1979 \times 10^{-09}$	$8.1475 \times 10^{-09}$	$2.6612 \times 10^{-09}$
0.900000	$4.7595 \times 10^{-10}$	$4.9371 \times 10^{-08}$	$3.5988 \times 10^{-08}$	$1.1516 \times 10^{-08}$
0.950000	$1.1847 \times 10^{-08}$	$2.1071 \times 10^{-07}$	$1.2450 \times 10^{-07}$	$3.9840 \times 10^{-08}$
1.000000	$1.1952 \times 10^{-07}$	$6.8526 \times 10^{-07}$	$3.5015 \times 10^{-07}$	$1.1361 \times 10^{-07}$
1.125000	$5.1861 \times 10^{-06}$	$6.5649 \times 10^{-06}$	$2.7484 \times 10^{-06}$	$9.4091 \times 10^{-07}$
1.156250	$1.0027 \times 10^{-05}$	$1.0202 \times 10^{-05}$	$4.1536 \times 10^{-06}$	$1.4455 \times 10^{-06}$
1.187500	$1.8013 \times 10^{-05}$	$1.5295 \times 10^{-05}$	$6.0903 \times 10^{-06}$	$2.1568 \times 10^{-06}$
1.218750	$3.0440 \times 10^{-05}$	$2.2195 \times 10^{-05}$	$8.6879 \times 10^{-06}$	$3.1285 \times 10^{-06}$
1.250000	$4.8980 \times 10^{-05}$	$3.1356 \times 10^{-05}$	$1.2097 \times 10^{-05}$	$4.4263 \times 10^{-06}$

TABLE IV. Superconducting temperatures  $T_c^{(\ell)}$  (in units of the Fermi temperature  $T_F$ ) for different  $r_s$  from RPA- $G^R$ . The symbol “—” indicates that the value of  $T_c$  is too small to be represented by a double-precision floating-point number.

$r_s$	$T_c^{(0)}$	$T_c^{(1)}$	$T_c^{(2)}$	$T_c^{(3)}$
0.337500	0	0	0	$1.848 \times 10^{-248}$
0.350000	0	0	0	$2.831 \times 10^{-181}$
0.356250	0	0	0	$5.646 \times 10^{-160}$
0.359375	0	0	0	$3.665 \times 10^{-151}$
0.362500	0	0	0	$2.615 \times 10^{-143}$
0.375000	0	0		$6.452 \times 10^{-119}$
0.381250	0	0		$1.003 \times 10^{-109}$
0.384375	0	0		$1.130 \times 10^{-105}$
0.387500	0	0	$1.366 \times 10^{-313}$	$6.269 \times 10^{-102}$
0.400000	0	0	$2.412 \times 10^{-207}$	$6.6615 \times 10^{-90}$
0.412500	0	0	$3.464 \times 10^{-153}$	$7.7736 \times 10^{-80}$
0.418750	0	0	$3.555 \times 10^{-136}$	$7.7817 \times 10^{-76}$
0.425000	0	0	$1.111 \times 10^{-122}$	$2.9707 \times 10^{-72}$
0.450000	0	0	$1.8986 \times 10^{-88}$	$4.9793 \times 10^{-61}$
0.456250	0	0	$8.2578 \times 10^{-83}$	$8.3200 \times 10^{-59}$
0.459375	0	0	$2.8627 \times 10^{-80}$	$9.1969 \times 10^{-58}$
0.462500	0	0	$6.8269 \times 10^{-78}$	$9.2354 \times 10^{-57}$
0.475000	0	0	$9.8906 \times 10^{-70}$	$3.9974 \times 10^{-53}$
0.500000	0		$4.3555 \times 10^{-58}$	$2.2543 \times 10^{-47}$
0.506250	0	$8.491 \times 10^{-282}$	$1.2004 \times 10^{-55}$	$5.0364 \times 10^{-46}$
0.509375	0	$9.489 \times 10^{-249}$	$1.4192 \times 10^{-54}$	$1.9576 \times 10^{-45}$
0.512500	0	$9.849 \times 10^{-223}$	$1.5107 \times 10^{-53}$	$7.3012 \times 10^{-45}$
0.525000	0	$1.667 \times 10^{-157}$	$7.6809 \times 10^{-50}$	$9.6863 \times 10^{-43}$
0.550000	0	$3.180 \times 10^{-100}$	$6.1712 \times 10^{-44}$	$3.7644 \times 10^{-39}$
0.575000	0	$3.8725 \times 10^{-74}$	$1.9191 \times 10^{-39}$	$3.1175 \times 10^{-36}$
0.587500	0	$8.6714 \times 10^{-66}$	$1.4080 \times 10^{-37}$	$5.7148 \times 10^{-35}$
0.590625	0	$5.2670 \times 10^{-64}$	$3.8236 \times 10^{-37}$	$1.1358 \times 10^{-34}$
0.593750	0	$2.5354 \times 10^{-62}$	$1.0101 \times 10^{-36}$	$2.2238 \times 10^{-34}$
0.600000	0	$2.6681 \times 10^{-59}$	$5.8416 \times 10^{-36}$	$7.2998 \times 10^{-34}$
0.650000	0	$7.7443 \times 10^{-43}$	$1.0118 \times 10^{-30}$	$4.8374 \times 10^{-30}$
0.675000	0	$7.4252 \times 10^{-38}$	$9.2698 \times 10^{-29}$	$1.5266 \times 10^{-28}$
0.687500	0	$7.9884 \times 10^{-36}$	$6.8043 \times 10^{-28}$	$7.2234 \times 10^{-28}$
0.690625	0	$2.3548 \times 10^{-35}$	$1.0932 \times 10^{-27}$	$1.0485 \times 10^{-27}$
0.693750	0	$6.7210 \times 10^{-35}$	$1.7405 \times 10^{-27}$	$1.5126 \times 10^{-27}$
0.700000	0	$4.7454 \times 10^{-34}$	$4.0702 \times 10^{-27}$	$2.9090 \times 10^{-27}$
0.750000	0	$1.5585 \times 10^{-28}$	$2.0370 \times 10^{-24}$	$4.5382 \times 10^{-25}$
0.800000	0	$8.5340 \times 10^{-25}$	$2.2287 \times 10^{-22}$	$2.3030 \times 10^{-23}$
0.850000	$9.797 \times 10^{-120}$	$4.6114 \times 10^{-22}$	$9.6861 \times 10^{-21}$	$6.0225 \times 10^{-22}$
0.900000	$5.7897 \times 10^{-58}$	$5.2413 \times 10^{-20}$	$1.9609 \times 10^{-19}$	$8.5010 \times 10^{-21}$
0.950000	$3.8577 \times 10^{-39}$	$2.2112 \times 10^{-18}$	$2.4495 \times 10^{-18}$	$8.2838 \times 10^{-20}$
0.953125	$2.2514 \times 10^{-38}$	$2.7177 \times 10^{-18}$	$2.8234 \times 10^{-18}$	$9.4232 \times 10^{-20}$
0.956250	$1.2216 \times 10^{-37}$	$3.3309 \times 10^{-18}$	$3.2494 \times 10^{-18}$	$1.0706 \times 10^{-19}$
0.962500	$2.9409 \times 10^{-36}$	$4.9637 \times 10^{-18}$	$4.2845 \times 10^{-18}$	$1.3767 \times 10^{-19}$
0.975000	$8.4522 \times 10^{-34}$	$1.0689 \times 10^{-17}$	$7.3212 \times 10^{-18}$	$2.2440 \times 10^{-19}$
1.000000	$9.0407 \times 10^{-30}$	$4.3732 \times 10^{-17}$	$1.9723 \times 10^{-17}$	$5.5433 \times 10^{-19}$
1.250000	$1.1905 \times 10^{-14}$	$3.8819 \times 10^{-13}$	$1.9591 \times 10^{-14}$	$3.7003 \times 10^{-16}$
1.375000	$4.8188 \times 10^{-12}$	$5.2926 \times 10^{-12}$	$1.6566 \times 10^{-13}$	$2.9358 \times 10^{-15}$
1.390625	$8.5285 \times 10^{-12}$	$6.9704 \times 10^{-12}$	$2.0832 \times 10^{-13}$	$3.6727 \times 10^{-15}$
1.406250	$1.4732 \times 10^{-11}$	$9.0872 \times 10^{-12}$	$2.6001 \times 10^{-13}$	$4.5643 \times 10^{-15}$

[1] J. Tuoriniemi, K. Juntunen-Nurmilaukas, J. Uusvuori, E. Pentti, A. Salmela, and A. Sebedash, Superconductivity in lithium below 0.4 millikelvin at ambient pressure, *Nature (London)* **447**, 187 (2007).

[2] O. Prakash, A. Kumar, A. Thamizhavel, and S. Ramakrishnan, Evidence for bulk superconductivity in pure bismuth single crystals at ambient pressure, *Science* **355**, 52 (2017).

[3] B. Uchoa and A. H. Castro Neto, Superconducting states of pure and doped graphene, *Phys. Rev. Lett.* **98**, 146801 (2007).

[4] R. Nandkishore, L. S. Levitov, and A. V. Chubukov, Chiral superconductivity from repulsive interactions in doped graphene, *Nat. Phys.* **8**, 158 (2012).

[5] M. Christos, S. Sachdev, and M. S. Scheurer, Correlated insulators, semimetals, and superconductivity in twisted trilayer graphene, *Phys. Rev. X* **12**, 021018 (2022).

[6] R. A. Ferrell, Fluctuations and the superconducting phase transition: II. Onset of Josephson tunneling and paraconductivity of a junction, *J. Low Temp. Phys.* **1**, 423 (1969).

[7] D. J. Scalapino, Pair tunneling as a probe of fluctuations in superconductors, *Phys. Rev. Lett.* **24**, 1052 (1970).

[8] J. T. Anderson and A. M. Goldman, Experimental determination of the pair susceptibility of a superconductor, *Phys. Rev. Lett.* **25**, 743 (1970).

[9] J. T. Anderson, R. V. Carlson, A. M. Goldman, and H.-T. Tan, The pair-field susceptibility of superconductors, in *Low Temperature Physics-LT 13: Volume 3: Superconductivity*, edited by K. D. Timmerhaus, W. J. O'Sullivan, and E. F. Hammel (Springer US, Boston, MA, 1974), pp. 709–714.

[10] N. Bergeal, J. Lesueur, M. Aprili, G. Faini, J. P. Contour, and B. Leridon, Pairing fluctuations in the pseudogap state of copper-oxide superconductors probed by the Josephson effect, *Nat. Phys.* **4**, 608 (2008).

[11] J.-H. She, B. J. Overbosch, Y.-W. Sun, Y. Liu, K. E. Schalm, J. A. Mydosh, and J. Zaanen, Observing the origin of superconductivity in quantum critical metals, *Phys. Rev. B* **84**, 144527 (2011).

[12] G. Koren and P. A. Lee, Observation of two distinct pairs fluctuation lifetimes and supercurrents in the pseudogap regime of cuprate junctions, *Phys. Rev. B* **94**, 174515 (2016).

[13] T. A. Maier and D. J. Scalapino, Pairfield fluctuations of a 2D Hubbard model, *npj Quantum Mater.* **4**, 30 (2019).

[14] A. Chubukov, N. V. Prokof'ev, and B. V. Svistunov, Implicit renormalization approach to the problem of Cooper instability, *Phys. Rev. B* **100**, 064513 (2019).

[15] X. Cai, T. Wang, N. V. Prokof'ev, B. V. Svistunov, and K. Chen, Superconductivity in the uniform electron gas: Irrelevance of the Kohn-Luttinger mechanism, *Phys. Rev. B* **106**, L220502 (2022).

[16] T. Wang, X. Cai, K. Chen, B. V. Svistunov, and N. V. Prokof'ev, Origin of the Coulomb pseudopotential, *Phys. Rev. B* **107**, L140507 (2023).

[17] N. N. Bogoljubov, V. V. Tolmachov, and D. V. Širkov, A new method in the theory of superconductivity, *Fortschr. Phys.* **6**, 605 (1958).

[18] M. Simonato, M. I. Katsnelson, and M. Rösner, Revised Tolmachev-Morel-Anderson pseudopotential for layered conventional superconductors with nonlocal Coulomb interaction, *Phys. Rev. B* **108**, 064513 (2023).

[19] A. Kapitulnik, S. A. Kivelson, and B. Spivak, *Colloquium: Anomalous metals: Failed superconductors*, *Rev. Mod. Phys.* **91**, 011002 (2019).

[20] H. Rietschel and L. J. Sham, Role of electron Coulomb interaction in superconductivity, *Phys. Rev. B* **28**, 5100 (1983).

[21] Y. Takada, Plasmon mechanism of superconductivity in two- and three-dimensional electron systems, *J. Phys. Soc. Jpn.* **45**, 786 (1978).

[22] Y. Takada, *s*- and *p*-wave pairings in the dilute electron gas: Superconductivity mediated by the Coulomb hole in the vicinity of the Wigner-crystal phase, *Phys. Rev. B* **47**, 5202 (1993).

[23] V. M. Galitski and S. Das Sarma, Kohn-Luttinger pseudopairing in a two-dimensional Fermi liquid, *Phys. Rev. B* **67**, 144520 (2003).

[24] Y. in 't Veld, M. I. Katsnelson, A. J. Millis, and M. Rösner, Screening induced crossover between phonon- and plasmon-mediated pairing in layered superconductors, [arXiv:2303.06220](https://arxiv.org/abs/2303.06220).

[25] W. Kohn and J. M. Luttinger, New mechanism for superconductivity, *Phys. Rev. Lett.* **15**, 524 (1965).

[26] X. Cai, T. Wang, P. Hou, Y. Deng, N. V. Prokof'ev, B. V. Svistunov, and K. Chen (unpublished).

[27] T. Büche and H. Rietschel, Superconductivity in the homogeneous electron gas: Exchange and correlation effects, *Phys. Rev. B* **41**, 8691 (1990).

[28] J. Kaye, K. Chen, and O. Parcollet, Discrete Lehmann representation of imaginary time Green's functions, *Phys. Rev. B* **105**, 235115 (2022).

[29] J. Kaye, K. Chen, and H. U. Strand, Libdlr: Efficient imaginary time calculations using the discrete Lehmann representation, *Comput. Phys. Commun.* **280**, 108458 (2022).

[30] <https://github.com/numericalEFT/ElectronGas.jl>. This is a link to the code of the linear response approach in this paper.

[31] R. L. Frank, C. Hainzl, S. Naboko, and R. Seiringer, The critical temperature for the BCS equation at weak coupling, *J. Geom. Anal.* **17**, 559 (2007).

[32] C. Hainzl and R. Seiringer, Critical temperature and energy gap for the BCS equation, *Phys. Rev. B* **77**, 184517 (2008).

[33] M. A. Baranov, A. V. Chubukov, and M. Yu. Kagan, Superconductivity and superfluidity in Fermi systems with repulsive interactions, *Intl. J. Mod. Phys. B* **06**, 2471 (1992).

[34] C. Frye and C. J. Efthimiou, Spherical harmonics in *p* dimensions, [arXiv:1205.3548](https://arxiv.org/abs/1205.3548).